



Highly enhanced stability and efficiency for atmospheric ammonia photocatalysis by hot electrons from a graphene composite catalyst with Al₂O₃



Yang Yang^{a, b}, Tengfei Zhang^{a, b}, Zhen Ge^{a, b}, Yanhong Lu^c, Huicong Chang^{a, b},
Peishuang Xiao^{a, b}, Ruiqi Zhao^{a, b}, Yanfeng Ma^{a, b}, Yongsheng Chen^{a, b, *}

^a The Centre of Nanoscale Science and Technology and Key Laboratory of Functional Polymer Materials, State Key Laboratory and Institute of Elemento-Organic Chemistry, Collaborative Innovation Center of Chemical Science and Engineering (Tianjin), College of Chemistry, Nankai University, Tianjin, 300071, China

^b School of Materials Science and Engineering, The National Institute for Advanced Materials, Nankai University, Tianjin, 300350, China

^c School of Chemistry & Material Science, Langfang Teachers University, Langfang, Hebei, 065000, China

ARTICLE INFO

Article history:

Received 17 May 2017

Received in revised form

3 July 2017

Accepted 5 July 2017

Available online 6 July 2017

ABSTRACT

Stable and cost-effective catalysts for efficient ammonia synthesis under mild conditions particularly at ambient pressure and temperature have been pursued widely and intensively. Recently we have reported a method using a composite catalyst with nano iron oxide hosted in a three-dimensional cross-linked graphene template material, Fe@3DGraphene. With this catalyst, a light driven and efficient ammonia synthesis from N₂ and H₂ directly at ambient pressure was achieved, where graphene works as an electron reservoir under light illumination. But, the catalytic activity dropped over time due to the aggregation of the Fe₂O₃ particles. Here we report the new version of this catalyst, a nano Al₂O₃ modified Fe@3DGraphene catalyst (Fe–Al@3DGraphene) through a simple solvothermal method, where nano Al₂O₃ serves as a barrier among nano Fe₂O₃ to efficiently prevent the aggregation of the Fe₂O₃ particles. The optimized ammonia synthesis rate of 430 μg g_{cat}⁻¹ h⁻¹ was achieved and kept steady for a 60-h test which was enhanced to more than twice of the previous catalyst without Al₂O₃ structural promoter.

© 2017 Elsevier Ltd. All rights reserved.

1. Introduction

Catalytic ammonia synthesis technology has played a central role in the development of the chemical industry during the 20th century [1–4]. This industrial significance has also been paralleled by tremendous studies for the mechanism [4–7] and the design of new and milder catalysts [8–10]. However, the industry catalytic ammonia synthesis process (Haber-Bosch process), as one of the most complicated and successful chemical engineering processes, is operated at both high temperature and pressure, mainly because of the extremely high bond energy (945 kJ mol⁻¹) and inert molecular structure of nitrogen molecule and the absence of

permanent dipole of the triple bond in nitrogen molecular [8,11]. Therefore, it has been a persistent challenge to achieve ammonia synthesis at milder conditions such as at ambient pressure and temperature together with an efficient and stable catalytic activity [2]. Among various strategies, the introduction of electrical, photo and radiation energies has been widely used to overcome the high energy barrier in the ammonia synthesis process [9,10,12–19].

Indeed, in the last entire century, great progresses have been made using various strategies such as electrical-catalysis [12–15,19], biological-catalysis [17,20,21] and photo-catalysis [10,18] for this paramount ammonia synthesis. For examples, an efficient electrochemical process with a rate of 2.4×10^{-9} mol s⁻¹ cm⁻² operated at 200 °C by the electrolysis of air and steam in molten sodium hydroxide with nano-Fe₂O₃ as the catalyst was reported by Licht et al. [9] Paul W. King found that cadmium sulfide (CdS) nanocrystals could be used to photosensitize the nitrogenase molybdenum-iron (MoFe) protein, and reached a rate of 315 ± 55 nmol NH⁺ (mg MoFe protein)⁻¹ min⁻¹ at a TOF of 75 min⁻¹ [17]. A unique photocatalytic approach based on

* Corresponding author. The Centre of Nanoscale Science and Technology and Key Laboratory of Functional Polymer Materials, State Key Laboratory and Institute of Elemento-Organic Chemistry, Collaborative Innovation Center of Chemical Science and Engineering (Tianjin), College of Chemistry, Nankai University, Tianjin, 300071, China.

E-mail address: yschen99@nankai.edu.cn (Y. Chen).

hot electron was also reported by our group recently [18]. In such an approach, a 3D cross-linked graphene based catalyst, Fe@3D-Graphene (Fe@3DG, Catalyst-I), hot (ejected) electrons from this composite catalyst induced by visible light, could efficiently facilitate the activation of N_2 and generate ammonia from N_2 and H_2 directly at ambient pressure with only light illumination. A mechanism was proposed that, under light illumination, graphene in such a catalyst works as an efficient electron emitter following an Auger-like light induced electron emission (LIEE) mechanism and the generated hot/free electrons work as the most powerful [22] and clean reducing agent to drive the reactions efficiently through several possible paths to facilitate the activation of N_2 molecules: 1) increasing the electron density at the Fe surface, 2) hot electron could be accepted by the anti-bond orbitals of N_2 adsorbed on Fe catalyst, 3) N_2 not adsorbed on Fe catalyst could be activated directly by accepting these ejected highly energetic electrons [23–25]. But one of the issues of such a catalyst is that the ammonia synthesis rate dropped significantly over time [18]. Obviously, such a problem has to be overcome for any possible practical application. This is also the case for the most well-known Haber-Bosch (HB) catalyst, where various morphology controlling additives have been developed to maintain the Fe catalytic activity, including the widely used heat-resisting structural promoter oxides such as Al_2O_3 , MgO and BaO etc. [11,26].

With this, the second generation catalyst, a Fe_2O_3 and graphene composite catalyst with Al_2O_3 (Fe–Al@3DG, Catalyst-II), was developed, where Al_2O_3 was used as the structural promoter to avoid the heating-induced aggregation of nano Fe_2O_3 uniformly dispersed in the 3D cross-linked bulk graphene template through a simple solvothermal method. Its catalytic activity kept steady for a 60-h test, compared with the significant activity drop (only 50% activity remained after 5 h) of the previous Catalyst-I without Al_2O_3 . An extra but also important benefit is that the catalytic activity of Catalyst-II is much enhanced to twice of that of best Catalyst-I under the same conditions. This is due to that Al_2O_3 , acting as a morphology controller, decreases the particle size of Fe_2O_3 in the Catalyst-II and thus increases the activity with the same iron loading.

2. Experimental

2.1. Materials synthesis

2.1.1. Synthesis of Catalyst-II: Fe–Al@3DGraphene (Fe–Al@3DG)

3DGraphene loaded with different weight of iron oxide (denoted as Fe–Al@3DG) were synthesized according to the literature procedures [18,23,24]. As a typical example, for the catalyst 20Fe–2Al@3DG, $Fe(NO_3)_3 \cdot 9H_2O$ (118.3 mg, 98%, J&K Technology Co., Ltd.) and $Al(NO_3)_3 \cdot 9H_2O$ (3.5 mg, 98%, J&K Technology Co., Ltd.) were dissolved in ethanol (30 mL) and then mixed with a GO ethanol dispersion (30 mL, 0.75 mg mL^{-1}) by stirring for 2 h. The mixed solution was sealed in a 100 mL Teflon-lined autoclave and heated up to $180 \text{ }^\circ\text{C}$ and maintained at this temperature for 12 h. The autoclave was then naturally cooled to room temperature. Then the as-prepared ethanol-filled intermediate product was carefully removed from the autoclave to have a slow and gradually solvent exchange with water. After the solvent exchange process was totally completed, the water-filled product was freeze-dried and then dried in a vacuum oven at $120 \text{ }^\circ\text{C}$ for 12 h. Finally, the sample was annealed at $450 \text{ }^\circ\text{C}$ in H_2/Ar (5/95, v/v) for 6 h, and denoted as Fe–Al@3DG (Catalyst-II). The final Fe and Al loading, by using atomic emission spectrometry with inductively coupled plasma (ICP-AES), was measured at 20 wt. % for Fe and 2 wt. % for Al (Table S1) thus denoted as 20Fe–2Al@3DG for convenience.

2.1.2. Synthesis of Catalyst-I: Fe@3DGraphene (Fe@3DG)

This reference iron oxide catalyst, denoted as Fe@3DG, was synthesized using the same solvothermal method as described above, $Fe(NO_3)_3 \cdot 9H_2O$ (118.3 mg, 98%, J&K Technology Co., Ltd.) was dissolved in ethanol (30 mL) and then mixed with a GO ethanol dispersion (30 mL, 0.75 mg mL^{-1}) by stirring for 2 h. The solution was then treated as the same solvothermal process of 3DG described above. The as-prepared ethanol-filled intermediate product was applied for a slow and gradually solvent exchange with water and then freeze-dried. The final product was obtained by the same annealing process as Catalyst-II.

2.2. Characterization

The structures of the samples were investigated by X-ray diffraction (XRD) performed on a Rigaku D/Max-2500 diffractometer with Cu $K\alpha$ radiation X-ray photoelectron spectroscopy (XPS) analysis was obtained using AXIS HIS 165 spectrometer (Kratos Analytical) with a monochromatized Al $K\alpha$ X-ray source (1486.7 eV) to analyze the chemical composition of the materials. Transmission electron microscopy (TEM) was carried out on a FEI Tecnai G2 microscope operated at an accelerating voltage of 300 kV. High angle annular dark field-scanning transmission electron microscopy (HAADF-STEM) and energy dispersive X-ray (EDX) mapping were carried out on a spherical aberration corrected transmission electron microscope (FEI Titan G2 80–200) which was operated at 200 kV. The UV–Vis diffuse reflectance spectra (UV–Vis DRS) were recorded by a Cary 5000 UV–visible–NIR spectrophotometer employing a lab-sphere diffuse reflectance accessory in the range of 220–2000 nm. Frequency histograms of iron oxide nanoparticle sizes and mean size were estimated with measured diameter from minimum 100 particles for each sample. The iron loading was determined by atomic emission spectrometry with inductively coupled plasma (ICP-AES) using ICP-9000 (N + M) apparatus (Thermo Jarrell-Ash Corp.) and the results are shown in Table S1.

2.3. Ammonia synthesis

2.3.1. Ammonia synthesis method

Reactions were carried out in the same reactor as our previous work shown in Fig. S1 (Supporting Information), and the catalyst, high pressure Hg lamp (500 W, Shanghai Jiguang Special Lighting Electrical Appliance Factory, Fig. S2, Supporting Information) and temperature probe were together placed in the center of the reactor and sealed, which was also surrounded by a water cooling jacket. The synthesis gas of H_2/N_2 (3/1, v/v) was flowed through the catalyst bed with a rate of 20 mL min^{-1} . The reaction was carried out at ambient pressure and the catalyst temperature was $\sim 200 \text{ }^\circ\text{C}$ due to the light heating. The gas-phase effluent was passed into a customized absorption bottle, which contains the diluted H_2SO_4 (60.00 mL , $0.0025 \text{ mol L}^{-1}$) to capture the ammonia produced, and then this absorption solution was analyzed by the indophenol blue method [10,18].

2.3.2. Ammonia measurement methods (The indophenol blue method)

This is following the literature [10,18]. A 2.00 mL absorption solution taken from the absorption bottle, was transferred to colorimetric tube and diluted to 10.00 mL with water. Then, an aqueous solution of $Na[Fe(NO)(CN)_5]$ ($100 \text{ } \mu\text{L}$, 1 wt %, Sigma-Aldrich), salicylic acid solution ($500 \text{ } \mu\text{L}$, 5 wt %, Sigma-Aldrich) and NaClO aqueous solution ($100 \text{ } \mu\text{L}$, 0.05 M, Tianjin Heowns Biochemical Technology Co., Ltd.) were in turn added to the absorption solution and homogeneously mixed. After 1 h standing at room temperature, the absorption spectrum was carried out using a

JASCO V-570 ultraviolet–visible spectrophotometer. The formation of indophenol blue was determined using the absorbance at the wavelength of 704 nm. Absolute calibration of the method was achieved using standard ammonium chloride solutions, prepared from the standard solid ammonium chloride (99.99%, Sigma-Aldrich).

2.3.3. Catalytic life time test

The ammonia product amount, measured using the indophenol blue method every 1 h, was used to demonstrate the activity of the catalyst as shown in Fig. 2c. Following the lamp requirement, the reaction (lamp) was turned off for every 3 h period.

2.3.4. Test with cut off UV light

With Xe lamp (500 W, Shanghai Jiguang Special Lighting Electrical Appliance Factory, Fig. S3) as the light source, a filter (its light transparency is shown in Fig. S4) was used to cut off the light below 400 nm of the Xe lamp. The reaction device was as shown in Fig. S5 with catalyst 20Fe–2Al@3DG (220 mg) and a temperature probe. The distance between the lamp and the reactor was adjusted to 2 cm and the filter was placed in the middle of the lamp and the reactor. The mixture of H_2/N_2 (3/1, v/v) was flowed through the

catalyst with a rate of 20 mL min^{-1} . The reaction was carried out at ambient and the system temperature was $\sim 200^\circ\text{C}$ due to the light heating. The product ammonia amount was measured with the indophenol blue method. The control experiment using Xe lamp without filter was studied under the same conditions.

3. Results and discussion

3.1. Synthesis and structural analyses

As illuminated in Fig. 1a, the Catalyst-II (Fe–Al@3DG), denoted for iron oxide and alumina loaded on the bulk three-dimensional cross-linked graphene (3DG) material developed recently [23–25], was obtained using $Fe(NO_3)_3 \cdot 9H_2O$, $Al(NO_3)_3 \cdot 9H_2O$ and graphene oxide (Fig. S6, Supporting Information) as the precursors through a simple and easily scalable solvothermal reaction followed by an annealing process (details in Experimental Section). The loading of the iron oxide and alumina onto the 3DG template was confirmed and characterized by scanning electron microscopy (SEM, Fig. 1b) and transmission electron microscopy (TEM, Fig. 1c), which indicate that the graphene sheets are cross-linked to form a honeycomb structure and the Fe_2O_3 and Al_2O_3 particles are

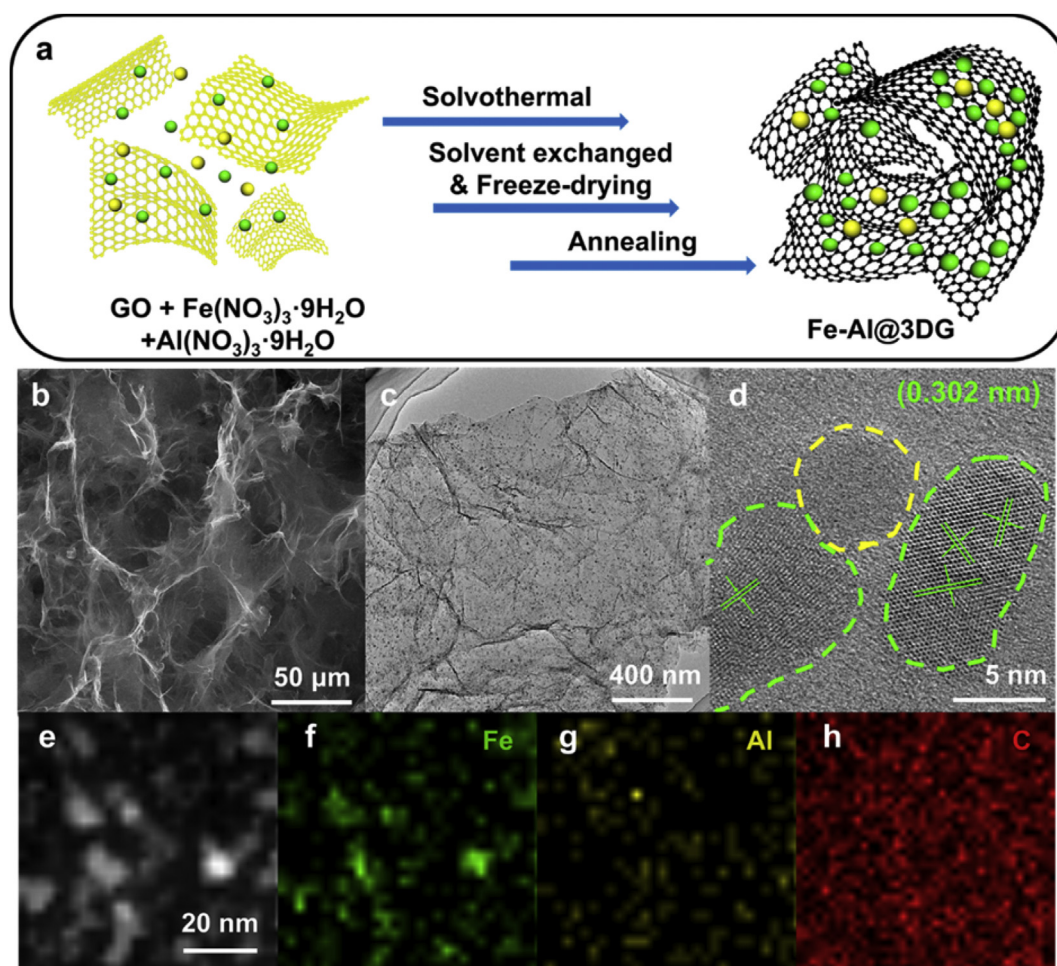


Fig. 1. Structural analyses of the Catalyst-II (Fe–Al@3DG). (a) Schematic illustration of the synthesis process of the Catalyst-II (Fe–Al@3DG). (b) SEM image and (c) TEM image of 20Fe–2Al@3DG. (d) HRTEM image of 20Fe–2Al@3DG. The ranges highlighted with green and yellow color circles show the iron oxide and alumina particles, respectively. The Al_2O_3 is added to form nanoparticles among the iron oxide particles like barrier and prevents the aggregation of iron oxide. The iron oxide lattice fringes are all at $\sim 0.302 \text{ nm}$ and correspond well to the cubic maghemite (220) plane. The alumina is amorphous in structure. (e–h) HAADF-STEM image and corresponding EDX maps of Fe–Al@3DG for Fe (f), Al (g) and C (h). (A colour version of this figure can be viewed online.)

homogeneously distributed on the graphene sheets among the void space. As shown in the high-resolution transmission electron microscopy (HRTEM) image (Fig. 1d), the existence and morphology of iron oxide and alumina particles in the catalyst were exhibited with the green and yellow color circles highlighted, respectively. The iron lattice fringes are all at ~ 0.302 nm and correspond well to the cubic maghemite (220) plane. And the Al_2O_3 nanoparticles were formed among the Fe_2O_3 particles and thus could act as a barrier to avoid further aggregation of Fe_2O_3 particles during the catalytic process. To further confirm the structure of Fe–Al@3DG, a HAADF–STEM image with sub-Angstrom resolution was carried out showing that both Fe_2O_3 and Al_2O_3 have been formed (Fig. 1d), and the corresponding EDX maps showed that the Fe_2O_3 and Al_2O_3 nanoparticles were also distributed homogeneously (Fig. 1e–g). More structural analyses of Fe–Al@3DG are illustrated in the Supporting Information (Figs. S7–9). The catalytic activity was measured using the same reactor as our previous work [18] containing the catalysts, where the mixture of H_2/N_2 (3/1, v/v) was flowed through the reactor with Hg lamp continuum light inside and water cooling outside (Fig. S1, Supporting information). Due to the light induced heating, while with vigorous cooling, the temperature inside the reactor was still at ~ 200 °C but kept roughly same for all the testing. The ammonia amount was quantitatively measured using an indophenol blue method [10,18].

3.2. Catalytic activity and lifetime test

While it is generally accepted that Al_2O_3 could work as the structural promoter as that in the HB catalyst, the best ratio is still yet to know. Thus, a series of catalysts with different Fe and Al loading ratios and composition were prepared and their catalytic activity was investigated under the same conditions. These included varying the Fe content with the same Fe/Al ratio (Fig. 2a) and altering the Fe/Al ratio with the fixed Fe content (Fig. 2b).

Generally, when Al_2O_3 acts as a structural promoter or support in composite catalysts, the mass ratio of the Fe (real metal catalyst) and Al varies from 30:1 to 1:10 [26–29]. At first, the mass ratio of Fe and Al was selected as 10:1 with different Fe contents (5%–30%), and the results were shown in Fig. 2a. It can be seen that the activity of the catalyst increases firstly with the increasing of Fe loading, and the best activity was achieved at 20 wt. % Fe and 2 wt. % Al loading (20Fe–2Al@3DG) with an average rate (3 h) of $430 \mu\text{g g}_{\text{cat}}^{-1} \text{h}^{-1}$. This is different from the Catalyst-I, where the best activity ($180 \mu\text{g g}_{\text{cat}}^{-1} \text{h}^{-1}$) was obtained for the catalyst with 7 wt. % Fe loading (7Fe@3DG). Then, with the increasing Fe loading, the ammonia synthesis rate dropped instead. With these results, the catalyst activity with different Fe/Al mass ratios varying from 20:1 to 20:10 but at a fixed Fe loading of 20 wt. % was further studied. It was found that the activity increased first and then decreased with

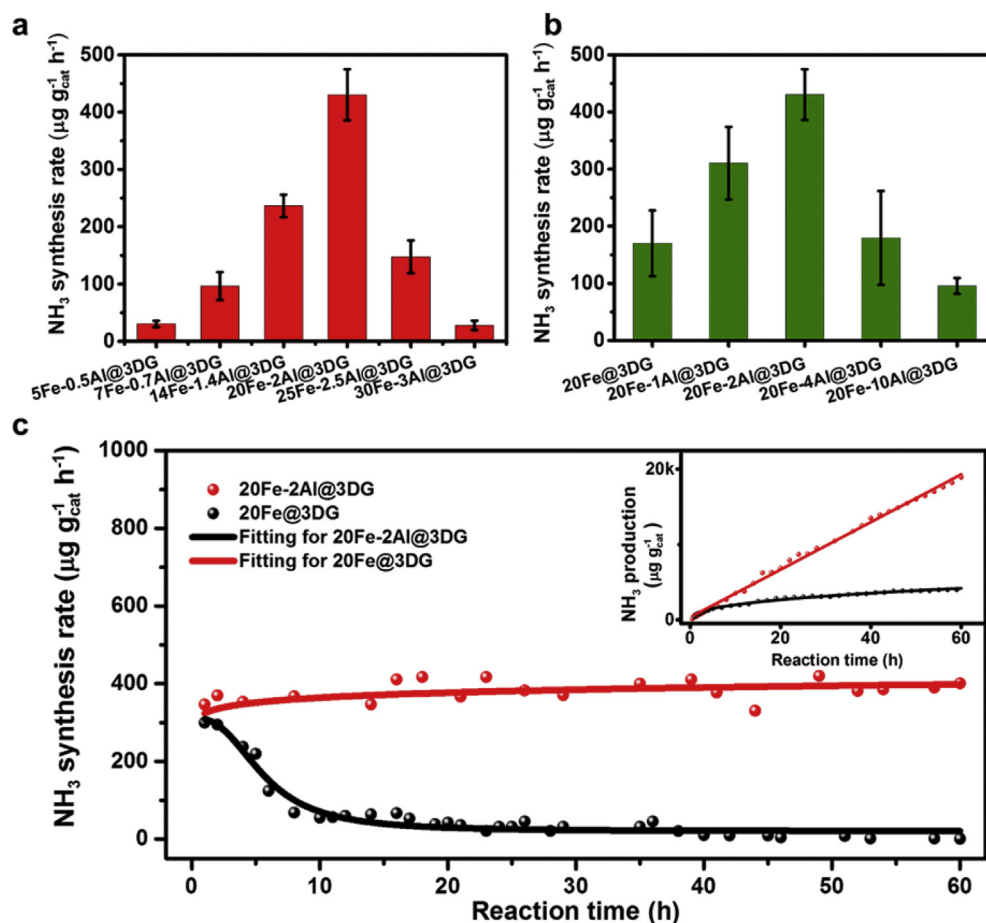


Fig. 2. Catalytic activity and stability test of Catalyst-I and Catalyst-II. (a) Ammonia synthesis rate vs different catalysts varying the iron contents with the same Fe and Al ratio (10:1). (b) Ammonia synthesis rate vs different catalysts altering Fe and Al ratio with the same iron loading of 20 wt. %. (c) The stability of the 20Fe–2Al@3DG and 20Fe@3DG. The activity of 20Fe–2Al@3DG remains steady in a 60-h test. In contrast, the activity of 20Fe@3DG drops after an hour, and it fell down to 10% of initial activity in 10 h. Inset, the overall ammonia production vs reaction time. (A colour version of this figure can be viewed online.)

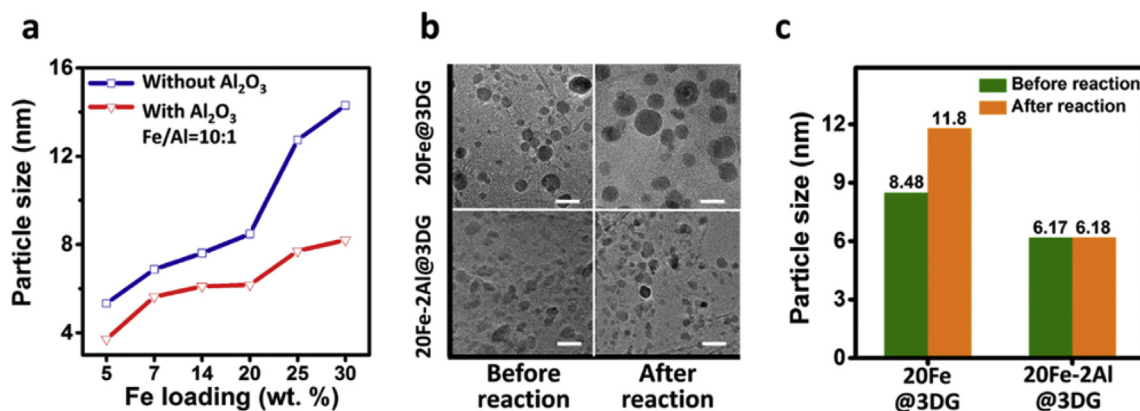


Fig. 3. Studies of the reason of highly enhanced efficiency and stability. (a) Particle size of different catalysts. The blue line shows the particle size of the Catalyst-I without Al₂O₃ increases significantly with the Fe loading. While for the Catalyst-II with the Al₂O₃ (Fe/Al = 10:1), not only the average particle size is smaller than that of the Catalyst-I under the same iron loading, but also the overall particle sizes of the Catalyst-II do not increase as much as that for the Catalyst-I. (b) The TEM image of Catalyst-I (20Fe@3DG) and Catalyst-II (20Fe-2Al@3DG) before and after reaction, respectively. Scale bar, 20 nm. (c) Particle size of 20Fe@3DG and 20Fe-2Al@3DG before and after reaction. For 20Fe-2Al@3DG, with the Al₂O₃ as the structural promoter to prevent the aggregation of iron, the particle size essentially remained the same before (6.17 nm) and after (6.18 nm) even a 60-h reaction. However, the particle size of 20Fe@3DG without Al₂O₃ dramatically increases from 8.48 nm to 11.80 nm after the reaction. (A colour version of this figure can be viewed online.)

further increasing Al loading (Fig. 2b). The highest activity of the Catalyst-II was obtained when the proportion of Fe and Al is 20:2 with 20 wt. % Fe loading. It is important to point out that this activity is nearly twice of that of the Catalyst-I without Al₂O₃ with the same Fe loading (20Fe@3DG, 170 μg g_{cat}⁻¹ h⁻¹).

The lifetime test was then carried out to evaluate the stability of the optimized Catalyst-II (20Fe-2Al@3DG) and Catalyst-I with the same Fe loading but without Al₂O₃ (20Fe@3DG), and the results were shown in Fig. 2c. For the catalyst 20Fe@3DG (black line), its catalytic activity dropped after 1 h, and fell to approximately 50% and 10% after 5 and 10 h, respectively. On the other hand, the high activity of the 20Fe-2Al@3DG (red line) was quite steady, and no significant activity decrease was observed even after a 60-h test, significantly improved compared with the catalyst without structural promoter.

3.3. Mechanism

It has been approved that the activity of the catalyst is dependent on the amount of the actual catalytic sites (active site/center) [6,29,30] on the nano-scale iron domain in the catalyst. In our previous work, the activity of the Catalyst-I (Fe@3DG) dropped (1) when the iron loading is further increased more than 7 wt. % and (2) after prolonged reaction time [18]. With increased iron loading, the size of iron oxide particles became larger and larger as shown in Fig. 3a (blue line) and Fig. S10. Thus, over increased iron loadings could reduce *specific* active site numbers of the catalysts, which decreases the overall activity. Similarly, in the case of prolonged reaction time, the dropped activity of Fe@3DG after 1 h could be attributed to the iron particle slow heat sintering and aggregation during the reaction (Fig. 3b and c), as observed commonly in both the HB [1,6,11,26] and other heterogeneous catalysts [9,31,32]. On the contrary, after adding the barrier-like nano Al₂O₃, both the ammonia synthesis activity (Fig. 2a and b) and the lifetime (Fig. 2c) of the Catalyst-II are highly improved.

To reveal the reasons of the highly enhanced efficiency and stability, a series of studies were carried out. From Fig. 3a, it can be seen clearly that not only the average particle size of Catalyst-II is smaller than that of the Catalyst-I under the same iron loading, but also the overall particle sizes of the Catalyst-II do not increase as much as that for the Catalyst-I when the Fe loading increases. The detailed TEM images and corresponding particle size data were

shown in Fig. S10. Thus, even with the same iron loading, the Al₂O₃ modified Catalyst-II (Fe-Al@3DG) exhibits much enhanced catalytic activity, due to its much smaller Fe₂O₃ particle size compared with that of the Catalyst-I (Fe@3DG). And, the iron loading of the best activity Catalyst-II is up to 20 wt. % in comparison to the only 7 wt. % iron loading for the Catalyst-I. Therefore, the best activity of Catalyst-II is more than twice of that of the best Catalyst-I. Understandably, excess of Al₂O₃ would lead to too many non-active sites and thus would decrease the overall activity [26]. So the best activity is achieved when the Fe/Al ratio is at 20:2.

The results for the morphology (Fig. 3b) and size distribution (Fig. 3c) before and after the reaction also reveal the reasons of the much enhanced lifetime of the Catalyst-II. Before the reaction, the particle size of 20Fe@3DG without Al₂O₃ is ~8.48 nm, and it increases significantly to ~11.80 nm after the reaction (Fig. 3c), leading the much declined activity. However, as shown in Fig. 3c, the particle size of Catalyst-II essentially remained the same before and after even a 60-h reaction. Thus, the initial Al₂O₃ particles dispersed uniformly among the iron act as a kind of barrier-like framework (Fig. 1c–g) and a structure/morphology keeper to prevent iron particles from sintering together. Meanwhile, XPS (Fig. S11, Supporting Information) and XRD (Fig. S12, Supporting Information) were used to investigate the chemical and structural properties of 20Fe-2Al@3DG after reaction, which showed that the structure and crystal plane were not changed.

Importantly, to confirm all photons from visible light could activate the reaction with Fe-Al@3DG, a control experiment was carried out using Xe lamp as the light source but with a light filter (cut off light below 400 nm completely, Supporting information). The result shows that a significant activity (~70%) still remained (Fig. S13, Supporting Information) without photons below 400 nm, indicating that the Catalyst-II (Fe-Al@3DG) catalyst still exhibits good activity even when visible light is used, though UV light might show the stronger activity as expected due to the higher photon energy [18].

4. Conclusion

In conclusion, the new version Catalyst-II (Fe-Al@3DG), with Al₂O₃ as structural promoter, demonstrated not only a much better lifetime but also a significantly enhanced catalytic activity for the ammonia synthesis (Fig. 4). The remarkable stability of such a

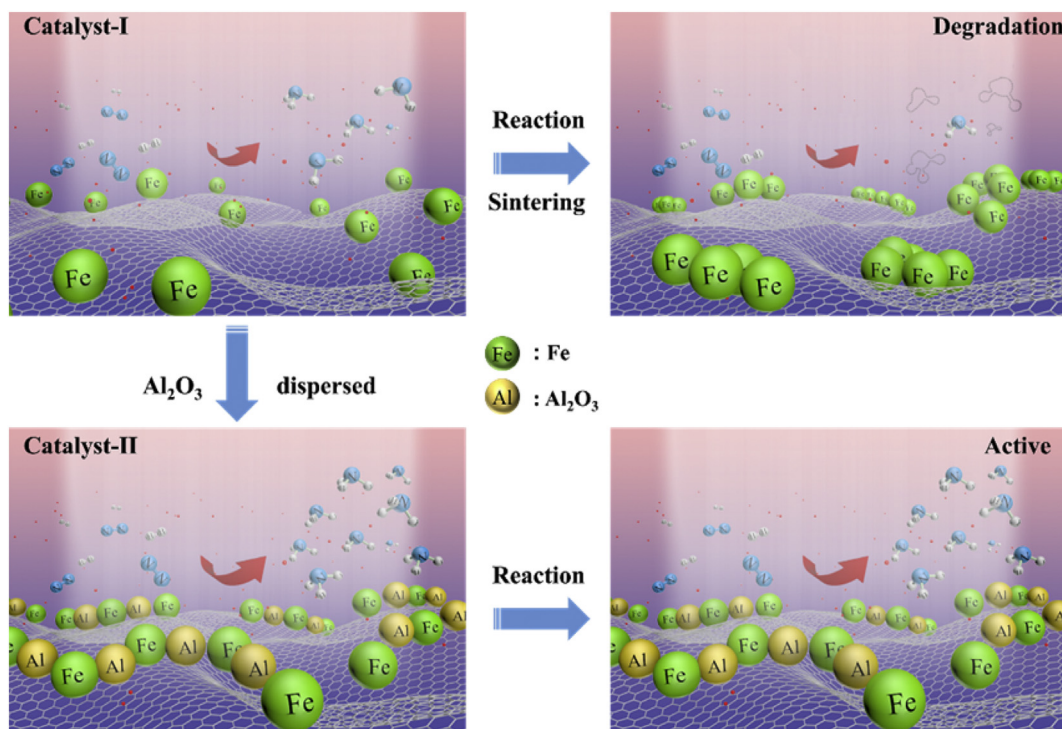


Fig. 4. Diagram of ammonia synthesis on Fe@3DG and Fe–Al@3DG. Without the addition of the Al₂O₃, the iron particles become aggregation after longtime reaction, and the activity decreases. While the Al₂O₃ plays an important role in the ammonia synthesis which can form a barrier to keep the iron particles from aggregation so that the activity keeps. (A colour version of this figure can be viewed online.)

catalyst was due to the prevention of iron particle aggregation during the reaction by the structural promoter Al₂O₃. Furthermore, with addition of Al₂O₃, the particle size of iron catalyst decreases significantly at the same iron loading and thus the overall activity gets increased. We expect this light-prompted catalysis might be applied to other reactions to increase the overall reaction efficiency.

Acknowledgements

The authors gratefully acknowledge the financial support from Ministry of Science and Technology of China (MoST, 2016YFA0200200), the National Natural Science Foundation of China (NSFC, 51633002 and 51472124).

Appendix A. Supplementary data

Supplementary data related to this article can be found at <http://dx.doi.org/10.1016/j.carbon.2017.07.014>.

References

- [1] G. Ertl, Reactions at surfaces: from atoms to complexity (Nobel Lecture), *Angew. Chem. Int. Ed.* 47 (19) (2008) 3524–3535.
- [2] R. Schlögl, Catalytic synthesis of ammonia—a “never-ending story”? *Angew. Chem. Int. Ed.* 42 (18) (2003) 2004–2008.
- [3] J.W. Erisman, M.A. Sutton, J. Galloway, Z. Klimont, W. Winiwarter, How a century of ammonia synthesis changed the world, *Nat. Geosci.* 1 (10) (2008) 636–639.
- [4] J.S. Anderson, J. Rittle, J.C. Peters, Catalytic conversion of nitrogen to ammonia by an iron model complex, *Nature* 501 (7465) (2013) 84–87.
- [5] B.M. Hoffman, D. Lukoyanov, Z.-Y. Yang, D.R. Dean, L.C. Seefeldt, Mechanism of nitrogen fixation by nitrogenase: the next stage, *Chem. Rev.* 114 (8) (2014) 4041–4062.
- [6] D. Strongin, The importance of C₇ sites and surface roughness in the ammonia synthesis reaction over iron, *J. Catal.* 103 (1) (1987) 213–215.
- [7] D.Y. Hwang, A.M. Mebel, Reaction mechanism of N₂/H₂ conversion to NH₃: a theoretical study, *J. Phys. Chem. A* 107 (16) (2003) 2865–2874.
- [8] H.P. Jia, E.A. Quadrelli, Mechanistic aspects of dinitrogen cleavage and hydrogenation to produce ammonia in catalysis and organometallic chemistry: relevance of metal hydride bonds and dihydrogen, *Chem. Soc. Rev.* 43 (2) (2014) 547–564.
- [9] S. Licht, B. Cui, B. Wang, F.F. Li, J. Lau, S. Liu, Ammonia synthesis. ammonia synthesis by N₂ and steam electrolysis in molten hydroxide suspensions of nanoscale Fe₂O₃, *Science* 345 (6197) (2014) 637–640.
- [10] D. Zhu, L.H. Zhang, R.E. Ruther, R.J. Hamers, Photo-illuminated diamond as a solid-state source of solvated electrons in water for nitrogen reduction, *Nat. Mater.* 12 (9) (2013) 836–841.
- [11] T. Kandemir, M.E. Schuster, A. Senyshyn, M. Behrens, R. Schlögl, The Haber-Bosch process revisited: on the real structure and stability of “ammonia iron” under working conditions, *Angew. Chem. Int. Ed.* 52 (48) (2013) 12723–12726.
- [12] G. Marnellos, M. Stoukides, Ammonia synthesis at atmospheric pressure, *Science* 282 (5386) (1998) 98–100.
- [13] T. Murakami, T. Nishikiori, T. Nohira, Y. Ito, Electrolytic synthesis of ammonia in molten salts under atmospheric pressure, *J. Am. Chem. Soc.* 125 (2) (2003) 334–335.
- [14] C.R. Dickson, A.J. Nozik, Nitrogen fixation via photoenhanced reduction on p-gallium phosphide electrodes, *J. Am. Chem. Soc.* 100 (25) (1978) 8007–8009.
- [15] R. Lan, J.T. Irvine, S. Tao, Synthesis of ammonia directly from air and water at ambient temperature and pressure, *Sci. Rep.* 3 (2013) 1145.
- [16] T. Oshikiri, K. Ueno, H. Misawa, Plasmon-induced ammonia synthesis through nitrogen photofixation with visible light irradiation, *Angew. Chem. Int. Ed.* 53 (37) (2014) 9802–9805.
- [17] K.A. Brown, D.F. Harris, M.B. Wilker, A. Rasmussen, N. Khadka, H. Hamby, et al., Light-driven dinitrogen reduction catalyzed by a CdS:nitrogenase MoFe protein biohybrid, *Science* 352 (6284) (2016) 448–450.
- [18] Y. Lu, Y. Yang, T. Zhang, Z. Ge, H. Chang, P. Xiao, et al., Photoprompted hot electrons from bulk cross-linked graphene materials and their efficient catalysis for atmospheric ammonia synthesis, *ACS Nano* 10 (11) (2016) 10507–10515.
- [19] X.T. Su, R.Q. Liu, J.D. Wang, Electrochemical properties of SrCe_{0.95}Y_{0.05}O₃-delta at intermediate temperature and its application to ammonia synthesis at atmospheric pressure, *Acta Chim. Sin.* 61 (4) (2003) 505–509.
- [20] A. Banerjee, B.D. Yuhua, E.A. Margulies, Y. Zhang, Y. Shim, M.R. Wasielewski, et al., Photochemical nitrogen conversion to ammonia in ambient conditions with FeMoS-chalcogels, *J. Am. Chem. Soc.* 137 (5) (2015) 2030–2034.
- [21] L.E. Roth, J.C. Nguyen, F.A. Tezcan, ATP- and iron-protein-independent activation of nitrogenase catalysis by light, *J. Am. Chem. Soc.* 132 (39) (2010) 13672–13674.
- [22] D. Brida, A. Tomadin, C. Manzoni, Y.J. Kim, A. Lombardo, S. Milana, et al., Ultrafast collinear scattering and carrier multiplication in graphene, *Nat.*

- Commun. 4 (2013) 1987.
- [23] Y. Wu, N. Yi, L. Huang, T. Zhang, S. Fang, H. Chang, et al., Three-dimensionally bonded spongy graphene material with super compressive elasticity and near-zero Poisson's ratio, *Nat. Commun.* 6 (2015) 6141.
- [24] T.F. Zhang, H.C. Chang, Y.P. Wu, P.S. Xiao, N.B. Yi, Y.H. Lu, et al., Macroscopic and direct light propulsion of bulk graphene material, *Nat. Phot.* 9 (7) (2015) 471–476.
- [25] Y. Lu, B. Ma, Y. Yang, E. Huang, Z. Ge, T. Zhang, et al., High activity of hot electrons from bulk 3D graphene materials for efficient photocatalytic hydrogen production, *Nano Res.* (2017) 1–11.
- [26] H. Liu, *Ammonia Synthesis Catalysts: Innovation and Practice*, Chemical Industry Press, 2013.
- [27] B. Lin, R. Wang, J. Lin, S. Du, X. Yu, K. Wei, Preparation of chlorine-free alumina-supported ruthenium catalyst for ammonia synthesis base on RuCl₃ by hydrazine reduction, *Catal. Commun.* 8 (11) (2007) 1838–1842.
- [28] B. Lin, R. Wang, J. Lin, J. Ni, K. Wei, Effect of carbon and chlorine on the performance of carbon-covered alumina supported Ru catalyst for ammonia synthesis, *Catal. Commun.* 12 (15) (2011) 1452–1457.
- [29] A. Miyazaki, I. Balint, K-i Aika, Y. Nakano, Preparation of Ru nanoparticles supported on γ -Al₂O₃ and its novel catalytic activity for ammonia synthesis, *J. Catal.* 204 (2) (2001) 364–371.
- [30] D. Gao, H. Zhou, J. Wang, S. Miao, F. Yang, G. Wang, et al., Size-dependent electrocatalytic reduction of CO₂ over Pd nanoparticles, *J. Am. Chem. Soc.* 137 (13) (2015) 4288–4291.
- [31] X. Guo, G. Fang, G. Li, H. Ma, H. Fan, L. Yu, et al., Direct, nonoxidative conversion of methane to ethylene, aromatics, and hydrogen, *Science* 344 (6184) (2014) 616–619.
- [32] C. Fernández, C. Sassoie, D.P. Debecker, C. Sanchez, P. Ruiz, Effect of the size and distribution of supported Ru nanoparticles on their activity in ammonia synthesis under mild reaction conditions, *Appl. Catal. A-Gen.* 474 (2014) 194–202.